

Role of noncollective excitations in low-energy heavy-ion reactions

S. Yusa,¹ K. Hagino,¹ and N. Rowley²¹*Department of Physics, Tohoku University, Sendai 980-8578, Japan*²*Institut de Physique Nucléaire, UMR 8608, CNRS-IN2P3 et Université de Paris Sud, F-91406 Orsay Cedex, France*

(Received 7 July 2010; published 10 August 2010)

We investigate the effect of single-particle excitations on heavy-ion reactions at energies near the Coulomb barrier. To this end, we describe single-particle degrees of freedom with the random matrix theory and solve the coupled-channels equations for one-dimensional systems. We find that the single-particle excitations hinder the penetrability at energies above the barrier, leading to a smeared barrier distribution. This indicates that the single-particle excitations provide a promising way to explain the difference in a quasielastic barrier distribution recently observed in $^{20}\text{Ne} + ^{90,92}\text{Zr}$ systems.

DOI: [10.1103/PhysRevC.82.024606](https://doi.org/10.1103/PhysRevC.82.024606)

PACS number(s): 24.10.Eq, 24.60.-k, 25.70.-z, 21.10.Pc

I. INTRODUCTION

Heavy-ion reactions near the Coulomb barrier provide a good opportunity to investigate an interplay between the reaction process and internal excitations in the colliding nuclei. For example, it is well known that sub-barrier fusion cross sections are significantly enhanced as compared to a prediction of a simple barrier penetration model because of the couplings of the relative motion between the colliding nuclei to nuclear intrinsic degrees of freedom [1–3]. It has been well recognized by now that the enhancement of fusion cross sections can be explained in terms of a distribution of Coulomb barrier heights originating from the couplings [4]. The barrier distribution can be actually extracted directly from the experimental data by taking the second derivative of the product of fusion cross section σ_{fus} and the center of mass energy E with respect to E , that is, $d^2[E\sigma_{\text{fus}}(E)]dE^2$ [4]. The experimental data have clearly shown that the barrier distribution makes a useful representation for understanding the reaction dynamics of heavy-ion sub-barrier fusion reactions [1,5].

A similar concept of barrier distribution has been applied also to heavy-ion quasielastic scattering (that is, a sum of elastic and inelastic scattering and transfer reactions) [6,7]. In this case, the barrier distribution is defined as the first derivative of the ratio of the quasielastic scattering cross section at a backward angle σ_{qel} to the Rutherford cross section σ_{R} , that is, $-d(\sigma_{\text{qel}}/\sigma_{\text{R}})/dE$. The fusion and quasielastic barrier distributions have been found to behave similarly to each other, at least in a qualitative way [6,8].

To analyze the sub-barrier enhancement of fusion cross sections and fusion and quasielastic barrier distributions, the coupled-channels method has been successfully employed. Typically, a few low-lying collective excitations are taken into account in a calculation [1,9]. With this approach, the barrier distribution arises naturally through the eigenchannel representation [1,10–12].

Recently, however, a few experimental data that cannot be accounted for by the conventional coupled-channels calculation have been obtained [13–17]. One of these examples is the quasielastic scattering experiment for the $^{20}\text{Ne} + ^{90,92}\text{Zr}$ systems [17]. The experimental data show that the quasielastic barrier distribution for these systems behaves in a significantly different way from each other: The barrier distribution for

the $^{20}\text{Ne} + ^{92}\text{Zr}$ system is much more smeared than that for the $^{20}\text{Ne} + ^{90}\text{Zr}$ system [17]. However, the coupled-channels calculations that take into account the collective rotational excitations in ^{20}Ne as well as the vibrational excitations in $^{90,92}\text{Zr}$ lead to similar barrier distributions for both systems because the strongly deformed ^{20}Ne nucleus mainly determines the barrier structure while the difference in the collective excitations in the two Zr targets plays a minor role. In Ref. [17], it was suggested that single-particle excitations in the colliding nuclei are responsible for smearing the barrier distribution for the $^{20}\text{Ne} + ^{92}\text{Zr}$ system. Notice that the single-particle excitations are expected to be much more important for the ^{92}Zr nucleus compared to the ^{90}Zr nucleus, which has the $N = 50$ shell closure. In fact, while there are only 12 states in the ^{90}Zr nucleus up to 4 MeV, there are 53 known states in the ^{92}Zr nucleus [18]. For 5 MeV, the number of known states is 35 and 87 for ^{90}Zr and ^{92}Zr , respectively (for another nucleus, ^{116}Sn , there are 81 known levels up to 3.9 MeV and 112 levels up to 4.3 MeV [19,20]).

The aim of this article is to investigate the effect of low-lying single-particle excitations on low-energy heavy-ion reactions, as conjectured in Ref. [17]. To understand qualitatively the effect of noncollective excitations, in this article we shall use a schematic model, that is, one-dimensional barrier penetration in the presence of the couplings to intrinsic degrees of freedom. The single-particle degrees of freedom can be described in several ways [21–26]. For instance, Ref. [21] used the Lindblad approach to discuss the role of quantum decoherence in deep sub-barrier hindrance of fusion cross sections. In this article, we employ the random matrix theory (RMT) to describe the single-particle excitations (see Refs. [27–30] for recent reviews on RMT). The random matrix approach for heavy-ion reactions was developed in 1970s by Weidenmüller and his collaborators to analyze heavy-ion deep inelastic collisions [22–25]. At that time, they derived the transport coefficients based on RMT [31] and solved the classical transport equations (see also Refs. [32,33]). The RMT has also been employed to discuss quantum dissipation [34–36]. In this article, instead of solving the classical equations, we directly solve the coupled-channels equations quantum mechanically by including the single-particle excitations described by RMT. Our approach is therefore similar to that in Ref. [26], in

which the coupled-channels equations with 200 dimension were solved for a one-dimensional model using a semiclassical approximation. In contrast to Ref. [26], we apply our formalism to the sub-barrier regime without using the semiclassical approximation. This will enable us to assess the effect of single-particle excitations on quantum tunneling and thus on the barrier distribution. By treating the single-particle states explicitly, we can also discuss the excitation spectra as a function of incident energy.

The article is organized as follows. In Sec. II, we detail the coupled-channels formalism with single-particle excitations described by RMT. In Sec. III, we apply the formalism to one-dimensional models for quantum tunneling. We discuss the effect of single-particle excitations on the barrier penetrability, the barrier distribution, and the excitation spectra. Using the results for the one-dimensional model, we also discuss the effect of noncollective excitations on quasielastic barrier distribution for the $^{20}\text{Ne} + ^{92}\text{Zr}$ system. We then summarize the article in Sec. IV.

II. FORMALISM

A. Coupled-channels method

The aim of this article is to discuss the effect of single-particle excitations on one-dimensional barrier penetrability. For this purpose, we assume the following Hamiltonian:

$$H = -\frac{\hbar^2}{2\mu} \frac{d^2}{dx^2} + V_{\text{rel}}(x) + H_0(\xi) + V_{\text{coup}}(x, \xi). \quad (1)$$

Here μ is the reduced mass and $V_{\text{rel}}(x)$ is a potential for the relative motion. $H_0(\xi)$ is a Hamiltonian for the intrinsic degrees of freedom of the colliding nuclei, and the last term, $V_{\text{coup}}(x, \xi)$, is a coupling Hamiltonian between the relative motion and the internal degrees of freedom.

The coupled-channels equations for this Hamiltonian are obtained by expanding the total wave function in terms of the eigenfunctions of $H_0(\xi)$ and read

$$\left\{ -\frac{\hbar^2}{2\mu} \frac{d^2}{dx^2} + V_{\text{rel}}(x) + \epsilon_n - E \right\} \psi_n(x) + \sum_m V_{nm}(x) \psi_m(x) = 0. \quad (2)$$

Here ϵ_n and $\psi_n(x)$ are the excitation energy and the wave function for the n th channel, respectively. $V_{nm}(x)$ is a coupling matrix and is a function of the coordinate x .

The coupled-channels equations are solved by imposing the boundary conditions of

$$\psi_n(x) \rightarrow \delta_{n,0} e^{-ik_0x} + r_n e^{ik_nx} \quad \text{for } x \rightarrow +\infty, \quad (3)$$

$$\rightarrow t_n e^{-ik_nx} \quad \text{for } x \rightarrow -\infty, \quad (4)$$

where $k_n = \sqrt{2\mu(E - \epsilon_n)/\hbar^2}$ is the wave number for the n th channel and 0 represents the entrance channel. We have assumed that the projectile is incident from the right-hand side of the potential barrier. With the transmission coefficients t_n , the penetration probability for the inclusive process is

calculated as

$$P(E) = \sum_n P_n(E) = \sum_n \frac{k_n}{k_0} |t_n|^2. \quad (5)$$

The barrier distribution is obtained by taking the derivative of $P(E)$, that is, $dP(E)/dE$ [11].

To take into account the single-particle excitations, as we show in the next section, one has to include a large number of channels. Because it is time and memory consuming to solve the coupled-channels equations with a large dimensionality, in this article we employ a constant coupling approximation [10]. In this approximation, the coupling matrix is assumed to be a constant over the whole range of x . Then one can diagonalize the matrix $A = (V_{nm} + \epsilon_n \delta_{n,m})$ with a coordinate independent unitary matrix U ,

$$UAU^\dagger = \text{diag}\{\lambda_1, \lambda_2, \dots\}, \quad (6)$$

where $\lambda_1, \lambda_2, \dots$, are the eigenvalues of A . Transforming the channel wave functions as

$$\tilde{\psi}_n(x) = \sum_m U_{nm} \psi_m(x), \quad (7)$$

the coupled-channels equations are transformed to a set of the uncoupled equations,

$$\left\{ -\frac{\hbar^2}{2\mu} \frac{d^2}{dx^2} + V_{\text{rel}}(x) + \lambda_n - E \right\} \tilde{\psi}_n(x) = 0. \quad (8)$$

We call the transformed channels the eigenchannels and, for each eigenchannel, $V_n(x) = V_{\text{rel}}(x) + \lambda_n$ the eigenpotential.

The boundary conditions for $\tilde{\psi}_n(x)$ are given by

$$\tilde{\psi}_n(x) \rightarrow U_{n0} e^{-ik_0x} + \tilde{r}_n e^{ik_0x} \quad \text{for } x \rightarrow +\infty \quad (9)$$

and

$$\tilde{\psi}_n(x) \rightarrow U_{n0} \tilde{t}_n e^{-ik_0x} \quad \text{for } x \rightarrow -\infty, \quad (10)$$

where the reflection and transmission coefficients are related to the original coefficients in Eqs. (3) and (4) by $\tilde{r}_n = \sum_m U_{nm} r_m / U_{n0}$ and $\tilde{t}_n = \sum_m U_{nm} t_m / U_{n0}$, respectively. Here we have assumed that the excitation energies are small compared to the incident energy so that k_n can be approximated by k_0 [10]. Using the coefficients \tilde{t}_n , the penetrability is calculated as

$$P(E) = \sum_n |U_{n0}|^2 |\tilde{t}_n(E)|^2. \quad (11)$$

The reflection coefficients in the original basis are given by

$$r_n = \sum_m (U^{-1})_{nm} U_{m0} \tilde{r}_m, \quad (12)$$

from which the Q -value distribution (that is, the excitation spectrum) is computed as

$$f(\epsilon) = \sum_n \frac{k_n}{k_0} |r_n|^2 \delta(\epsilon - \epsilon_n) \sim \sum_n |r_n|^2 \delta(\epsilon - \epsilon_n). \quad (13)$$

B. Coupling matrix elements

We solve the coupled-channels equations Eq. (2) using the constant coupling approximation by including both collective

and noncollective excitations. For the collective excitations, we assume either the vibrational or the rotational couplings. The coupling matrix for the vibrational coupling is given by

$$(V_{nm}) = F \begin{pmatrix} 0 & 1 \\ 1 & 0 \end{pmatrix}, \quad (14)$$

if we truncate the phonon space up to 1-phonon state [9]. Here F is a coupling constant, and we have assumed linear coupling. For rotational coupling, the coupling matrix is given by

$$(V_{nm}) = \frac{F_2}{\sqrt{4\pi}} \begin{pmatrix} 0 & 1 & 0 \\ 1 & \frac{2\sqrt{5}}{7} & \frac{6}{7} \\ 0 & \frac{6}{7} & \frac{20\sqrt{5}}{77} \end{pmatrix} + \frac{F_4}{\sqrt{4\pi}} \begin{pmatrix} 0 & 0 & 1 \\ 0 & \frac{6}{7} & \frac{20\sqrt{5}}{77} \\ 1 & \frac{20\sqrt{5}}{77} & \frac{486}{1001} \end{pmatrix} \quad (15)$$

up to the 4^+ state in the rotational band [9], where F_2 and F_4 are the quadrupole and hexadecapole coupling strengths, respectively.

For the single-particle excitations, we consider an ensemble of coupling matrix elements based on the RMT [22–24]. We assume that the matrix elements are uncorrelated random numbers obeying a Gaussian distribution with zero mean. That is, we require that the first and the second moments of the coupling matrix elements satisfy the following equations [37]:

$$\overline{V_{nm}(x)} = 0, \quad (16)$$

$$\overline{V_{rs} V_{nm}} = (\delta_{r,n} \delta_{s,m} + \delta_{r,m} \delta_{s,n}) g_{nm}, \quad (17)$$

$$g_{nm} = \frac{w_0}{\sqrt{\rho(\epsilon_n) \rho(\epsilon_m)}} e^{-\frac{(\epsilon_n - \epsilon_m)^2}{2\Delta^2}}, \quad (18)$$

where the overbar denotes an ensemble average and $\rho(\epsilon)$ is the nuclear level density. Here, we have assumed the coordinate independent matrix elements according to the constant coupling approximation.

For the single-particle excitations, we generate the coupling matrix elements according to these equations many times. For each coupling matrix, we do not vary the matrix elements for the collective excitations, which are uniquely determined once the coupling is specified. For each coupling matrix, we solve the coupled-channels equations and calculate the penetrability and the reflection probability. The physical results are then obtained by taking an average of these quantities.

In the actual calculations shown in the next section, we discretize the quasicontinuum single-particle spectrum in the coupled-channels equations [38,39] (see also Ref. [40]). Introducing the level density $\rho(\epsilon)$,

$$\rho(\epsilon) = \sum_n \delta(\epsilon - \epsilon_n), \quad (19)$$

the coupled-channels equation can be written in the following form:

$$\left\{ -\frac{\hbar^2}{2\mu} \frac{d^2}{dx^2} + V_{\text{rel}}(x) + \epsilon_n - E \right\} \psi_n(x) + \int d\epsilon \rho(\epsilon) V_{n\epsilon}(x) \psi_\epsilon(x) = 0. \quad (20)$$

In this equation, we assume a quasicontinuum spectrum for the single-particle excited states, and discretize the integral with a constant energy spacing, $\Delta\epsilon$. For the ground-state and the collective excitation channels, we then obtain

$$\left\{ -\frac{\hbar^2}{2\mu} \frac{d^2}{dx^2} + V_{\text{rel}}(x) + \epsilon_n - E \right\} \psi_n(x) + \sum_{m \notin \text{sp}} V_{nm}(x) \psi_m(x) + \sum_{m \in \text{sp}} \Delta\epsilon \rho(\epsilon_m) V_{n\epsilon_m}(x) \psi_{\epsilon_m}(x) = 0, \quad (21)$$

while for the single-particle channels denoted by ϵ_n we obtain

$$\left\{ -\frac{\hbar^2}{2\mu} \frac{d^2}{dx^2} + V_{\text{rel}}(x) + \epsilon_n - E \right\} \psi_{\epsilon_n}(x) + \sum_{m \notin \text{sp}} V_{\epsilon_n m}(x) \psi_m(x) + \sum_{m \in \text{sp}} \Delta\epsilon \rho(\epsilon_m) V_{\epsilon_n \epsilon_m}(x) \psi_{\epsilon_m}(x) = 0. \quad (22)$$

Here, $m \notin \text{sp}$ denotes a summation over the ground state and the collective channels, while $m \in \text{sp}$ is a summation over the single-particle channels. These equations can be expressed in a simpler way by multiplying a factor $\sqrt{\rho(\epsilon_n) \Delta\epsilon}$ for each index ϵ_n representing the single-particle channels. That is,

$$\tilde{\psi}_{\epsilon_n}(x) = \sqrt{\rho(\epsilon_n) \Delta\epsilon} \psi_{\epsilon_n}(x), \quad (23)$$

$$\tilde{V}_{n\epsilon_m}(x) = \sqrt{\rho(\epsilon_m) \Delta\epsilon} V_{n\epsilon_m}(x), \quad (24)$$

$$\tilde{V}_{\epsilon_n \epsilon_m}(x) = \Delta\epsilon \sqrt{\rho(\epsilon_n) \rho(\epsilon_m)} V_{\epsilon_n \epsilon_m}(x). \quad (25)$$

With these wave functions and the coupling matrix elements, Eqs. (21) and (22) read

$$\left\{ -\frac{\hbar^2}{2\mu} \frac{d^2}{dx^2} + V_{\text{rel}}(x) + \epsilon_n - E \right\} \psi_n(x) + \sum_{m \notin \text{sp}} V_{nm} \psi_m(x) + \sum_{m \in \text{sp}} \tilde{V}_{n\epsilon_m}(x) \tilde{\psi}_{\epsilon_m}(x) = 0, \quad (26)$$

and

$$\left\{ -\frac{\hbar^2}{2\mu} \frac{d^2}{dx^2} + V_{\text{rel}}(x) + \epsilon_n - E \right\} \tilde{\psi}_{\epsilon_n}(x) + \sum_{m \notin \text{sp}} \tilde{V}_{\epsilon_n m} \psi_m(x) + \sum_{m \in \text{sp}} \tilde{V}_{\epsilon_n \epsilon_m}(x) \tilde{\psi}_{\epsilon_m}(x) = 0, \quad (27)$$

respectively. From Eqs. (3) and (4), the boundary conditions for $\tilde{\psi}_{\epsilon_n}(x)$ are given by

$$\tilde{\psi}_{\epsilon_n}(x) \rightarrow \sqrt{\rho(\epsilon_n) \Delta\epsilon} t_n e^{-ik_n x} = \tilde{t}_n e^{-ik_n x} \quad \text{for } x \rightarrow -\infty \quad (28)$$

and

$$\tilde{\psi}_{\epsilon_n}(x) \rightarrow \sqrt{\rho(\epsilon_n) \Delta\epsilon} r_n e^{ik_n x} = \tilde{r}_n e^{ik_n x} \quad \text{for } x \rightarrow +\infty, \quad (29)$$

where, $\tilde{t}_n = \sqrt{\rho(\epsilon_n)\Delta\epsilon} t_n$ and $\tilde{r}_n = \sqrt{\rho(\epsilon_n)\Delta\epsilon} r_n$. The penetrability is then given by

$$\begin{aligned} P(E) &= \sum_{n \notin \text{sp}} \frac{k_n}{k_0} |t_n|^2 + \sum_{n \in \text{sp}} \frac{k_n}{k_0} \rho(\epsilon_n) \Delta\epsilon |t_n|^2 \\ &= \sum_{n \notin \text{sp}} \frac{k_n}{k_0} |t_n|^2 + \sum_{n \in \text{sp}} \frac{k_n}{k_0} |\tilde{t}_n|^2. \end{aligned} \quad (30)$$

This method with a constant energy step considerably reduces the computation time as compared to the case of treating the exponentially increasing number of single-particle levels as they are. It also validates the use of the RMT. An important assumption in RMT is that the ensemble average of a quantity is equivalent to the energy average of that quantity over the spectrum [28]. In our case, we expect that the ensemble average of the calculated results corresponds to the energy average of the same quantities within the energy spacing of $\Delta\epsilon$.

III. RESULTS

A. Vibrational coupling

We now numerically solve the coupled-channels equations and discuss the effect of single-particle excitations on barrier penetrability. We first consider the vibrational coupling. We assume that there is a collective vibrational state at 1 MeV whose coupling to the ground state is given by Eq. (14) with $F = 2$ MeV. For the single-particle states, we consider a level density given by $\rho(\epsilon) = \rho_0 e^{2\sqrt{a\epsilon}}$ with $\rho_0 = 0.039$ MeV⁻¹ and $a = 29/8$ MeV⁻¹, starting from 2 MeV. The value of ρ_0 was determined so that the number of single-particle levels is 200 up to 5 MeV. For the parameters for the couplings in Eq. (18), we follow Ref. [37] to use $\Delta = 7$ MeV. We arbitrarily choose the coupling strength to be $w_0 = 0.005$ MeV. The energy spectrum for this model is shown in Fig. 1. For the potential for the relative motion, $V_{\text{rel}}(x)$, we use a Gaussian

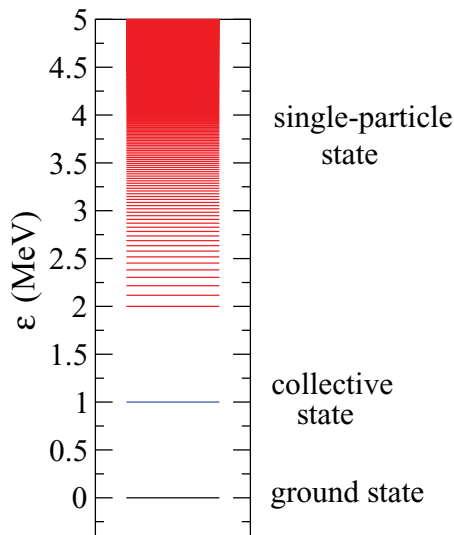


FIG. 1. (Color online) The energy spectrum for the model calculation we employ. There is a collective vibrational state at 1 MeV, while single-particle states exist from 2 MeV with an exponentially increasing level density.

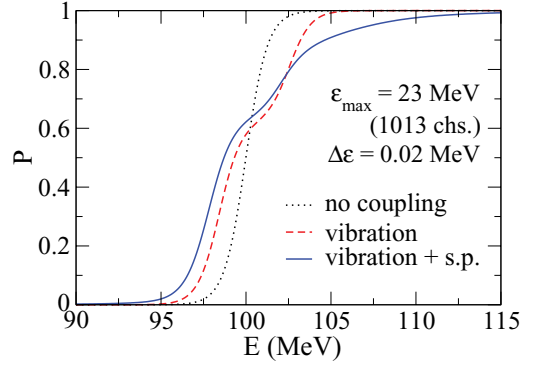


FIG. 2. (Color online) The potential penetrability obtained with several methods. The dotted line is obtained without channel coupling, while the dashed line takes into account only the collective vibrational excitation. The solid line shows the result with both the collective and the single-particle excitations.

function

$$V_{\text{rel}}(x) = V_B e^{-\frac{x^2}{2s_0^2}}, \quad (31)$$

with $V_B = 100$ MeV and $s_0 = 3$ fm [10]. The reduced mass μ is taken to be $29m_N$, m_N being the nucleon mass.

Figure 2 shows the penetrabilities thus obtained. The corresponding barrier distributions are shown in Fig. 3. The dotted and the dashed lines show the results without the channel couplings and those only with the collective excitation, respectively. The solid line shows the results with both the single-particle excitations and the collective excitation. We include the single-particle states up to $\epsilon_{\text{max}} = 23$ MeV with energy spacing of $\Delta\epsilon = 0.02$ MeV. With this model space, the number of channels included is 1013 (we treat the low-lying single-particle states as discrete states when the energy spacing is larger than $\Delta\epsilon$). This result is obtained by generating the coupling matrix elements 30 times to take an ensemble average. We have found that the fluctuation around the average is small. For instance, at $E = 100$ MeV, the averaged penetrability is $P = 0.622$, whereas the root-mean-square deviation is 4.366×10^{-3} . As we mentioned in the previous section, the results shown in Fig. 2 are obtained with the constant coupling approximation. With a smaller value of ϵ_{max} , we have solved the coupled-channels equations exactly

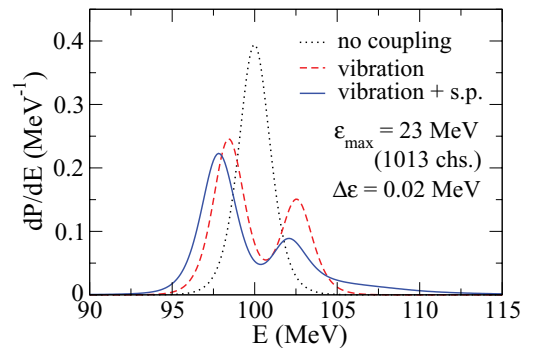


FIG. 3. (Color online) The barrier distribution defined by the first derivative of the penetrability. The meaning of each line is the same as in Fig. 2.

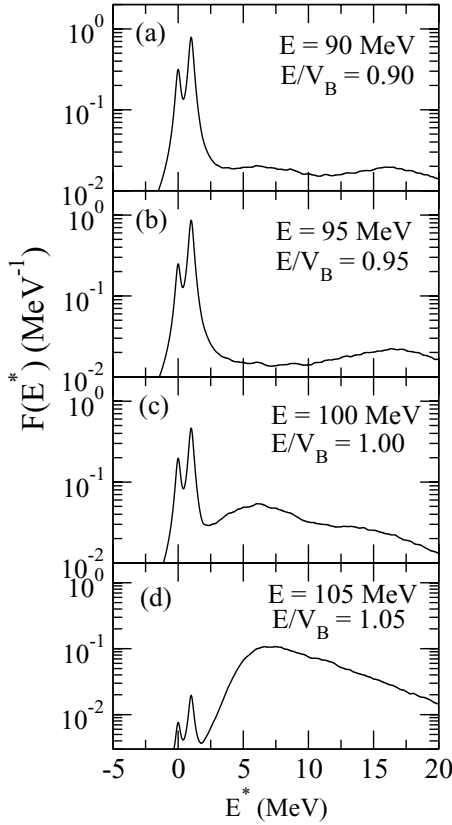


FIG. 4. The Q -value distribution for the reflected flux at four energies as indicated in the figure. It is obtained by smearing the discrete distribution with a Lorentzian function with the width of 0.2 MeV. The peaks at $E^* = 0$ and 1 MeV correspond to the elastic and the collective excitation channels, respectively.

and have confirmed that the constant coupling approximation works qualitatively well.

The collective excitation leads to a double-peaked structure of barrier distribution. One can see that the single-particle excitations suppress the penetrability at energies above the barrier and at the same time smear the higher energy peak in the barrier distribution, although the main structure of the barrier distribution is still determined by the collective excitation. The single-particle excitations also lower the barrier and thus increase the penetrability at energies below the barrier, owing to the well-known potential renormalization [41].

The Q -value distribution for the reflected flux is shown in Fig. 4 at four incident energies indicated in the figure. For presentation purposes, we fold the discrete distribution with a Lorentz function,

$$g(\epsilon) = \frac{1}{\pi} \frac{\eta}{\epsilon^2 + \eta^2}, \quad (32)$$

with the width of $\eta = 0.2$ MeV. That is, with the function defined by Eq. (13), we compute

$$F(E^*) = \int d\epsilon f(\epsilon) g(E^* - \epsilon) = \sum_n |r_n|^2 \frac{1}{\pi} \frac{\eta}{(E^* - \epsilon_n)^2 + \eta^2}. \quad (33)$$

In the figure, the peaks at $E^* = 0$ MeV and $E^* = 1$ MeV correspond to the elastic channel and the collective excitation channel, respectively. One can see that at energies well below the barrier the elastic and the collective peaks dominate in the distribution. As the energy increases, the single-particle excitations become more and more important. This behavior is consistent with the experimental Q -value distribution observed for $^{16}\text{O} + ^{208}\text{Pb}$ [42,43] and $^{16}\text{O} + ^{184}\text{W}$ [43] reactions. At energies above the barrier, the single-particle contribution is even larger than the contribution of the elastic and the collective peaks.

B. Rotational coupling

Let us next consider the rotational coupling. For this purpose, we mock up the $^{20}\text{Ne} + ^{92}\text{Zr}$ system. That is, we consider the rotational excitations in ^{20}Ne up to the 4^+ state and the single-particle excitations in ^{92}Zr . The energies of the rotational states are thus $\epsilon_{2^+} = 1.634$ MeV and $\epsilon_{4^+} = 4.248$ MeV for the 2^+ and 4^+ states, respectively. The values of the coupling strengths F_2 and F_4 in Eq. (15) are estimated with the collective model for the coupling form factor at the barrier position with the deformation parameters of $\beta_2 = 0.46$ and $\beta_4 = 0.27$. This yields $F_2 = -6.892$ MeV and $F_4 = -4.632$ MeV. For the single-particle excitations in ^{92}Zr , we consider the energy range of $2 \text{ MeV} \leq \epsilon \leq 16 \text{ MeV}$, with the exponential level density with $\rho_0 = 0.034 \text{ MeV}^{-1}$ and $a = 30/8 \text{ MeV}^{-1}$. For the coupling strength, we use $w_0 = 0.005 \text{ MeV}$ and $\Delta = 4.0 \text{ MeV}$. These parameters are adjusted so that the rotational excitation in ^{20}Ne gives the main structure of the barrier distribution.

In the calculation shown in what follows, we also include the mutual excitations of the projectile and the target nuclei. To avoid closed channels, we introduce the energy cutoff and include those channels whose total excitation energy is below 16 MeV. With this setup, the number of channels included is 1688.

We use the Gaussian function for the potential for the relative motion with $V_B = 51.76 \text{ MeV}$ and $s_0 = 2.475 \text{ fm}$. This yields the same barrier height and the curvature as those with a Woods-Saxon potential with the parameters of $V_0 = 59.9 \text{ MeV}$, $r_0 = 1.2 \text{ fm}$, and $a = 0.63 \text{ fm}$ for the $^{20}\text{Ne} + ^{92}\text{Zr}$ system. The reduced mass is taken to be $20 \times 92 m_N / 112$.

Figures 5 and 6 show the penetrability and the barrier distribution for this model, respectively. The meaning of each line is the same as in Figs. 2 and 3 for the vibrational coupling. With only the collective rotational excitations, there are three eigenbarriers whose heights are 48.2, 53.3, and 55.6 MeV. In contrast to the vibrational coupling, for the rotational coupling with a prolate deformation the main peak in the barrier distribution is not the lowest energy peak. For the parameters we use, the highest energy barrier carries a relatively small weight and the barrier distribution has only two visible peaks. The effect of single-particle excitations on the barrier distribution is similar to the case for the vibrational coupling and smears the higher energy peak in the barrier distribution.

C. Quasielastic barrier distribution

Using the eigenbarriers and the corresponding weight factors obtained in the previous subsection, one can compute

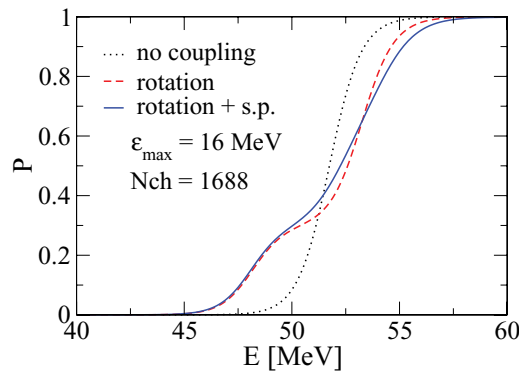


FIG. 5. (Color online) The same as Fig. 2, but for the rotational coupling.

the quasielastic scattering cross sections and the quasielastic barrier distribution in a three-dimensional space. That is, in the eigenchannel representation, the quasielastic scattering cross section is given by [7,44]

$$\sigma_{\text{qel}}(E, \theta) = \sum_i w_i \sigma_{\text{el}}(E - \lambda_i, \theta), \quad (34)$$

where $w_i = |U_{i0}|^2$ is the weight factor for the i th eigenchannel and σ_{el} is the elastic scattering cross section. To calculate the elastic scattering cross sections, we use the Woods-Saxon potential indicated in the previous section. For the imaginary part of the optical potential, we assume an internal absorption, in which the imaginary part is well localized only inside the Coulomb barrier.

Figure 7 shows the quasielastic barrier distribution obtained with the same w_i and λ_i as in the previous subsection for the one-dimensional model. We use the point difference formula with $\Delta E_{\text{c.m.}} = 2$ MeV to calculate the quasielastic barrier distribution. The meaning of each line is the same as in Fig. 3. Because the quasielastic barrier distribution is by itself smeared more than the fusion barrier distribution [7], and also because we use the point difference formula rather than taking the derivative, the higher energy peak in the barrier distribution is more smeared by the single-particle excitations as compared to the one-dimensional calculation

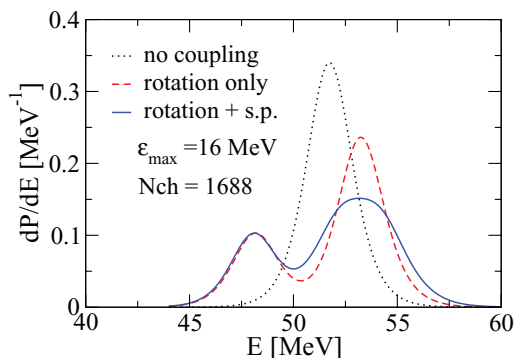


FIG. 6. (Color online) The same as Fig. 3, but for the rotational coupling.

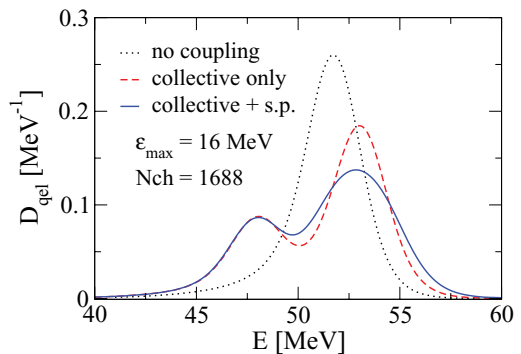


FIG. 7. (Color online) The quasielastic barrier distribution for the $^{20}\text{Ne} + ^{92}\text{Zr}$ system calculated with the weight factors and the eigenbarrier heights for the one-dimensional rotational model discussed in Sec. III B. The meaning of each line is the same as in Fig. 3.

shown in the previous section. The difference between the dashed line (the collective excitations only) and the solid line (the collective + single-particle excitations) is similar to the difference in the experimental quasielastic barrier distribution between $^{20}\text{Ne} + ^{90}\text{Zr}$ and $^{20}\text{Ne} + ^{92}\text{Zr}$ systems. We therefore conclude that the single-particle excitations indeed provide a promising way to explain the difference in the quasielastic barrier distribution for the $^{20}\text{Ne} + ^{90,92}\text{Zr}$ systems.

IV. SUMMARY

We have studied the role of single-particle excitations in heavy-ion reactions at energies close to the Coulomb barrier. To this end, we employed a RMT to describe the single-particle degrees of freedom. We applied the model to one-dimensional barrier-penetration problems by using the constant coupling approximation. In addition to the single-particle excitations, we also included the collective excitations with either a vibrational or a rotational character. We calculated the potential penetrability, the barrier distribution, and the Q -value distribution. We also calculated the quasielastic barrier distribution for the $^{20}\text{Ne} + ^{92}\text{Zr}$ system using the eigenbarriers and their weight factors obtained with the one-dimensional model. Our calculations show that the single-particle excitations hinder the penetrability at energies above the barrier and smear the high-energy part of the barrier distribution. In the Q -value distribution, we found that the contribution from the single-particle excitations increases significantly as the incident energy increases.

The experimental quasielastic barrier distributions are considerably different between $^{20}\text{Ne} + ^{90,92}\text{Zr}$ systems, despite that the coupled-channels calculations with collective excitations in the colliding nuclei lead to similar barrier distributions to each other. Our calculations imply that the difference can be indeed accounted for by the noncollective excitations in the target nuclei, as has been conjectured in Ref. [17]

To make a quantitative comparison to the experimental data and draw a definite conclusion on the quasielastic barrier

distribution for the $^{20}\text{Ne} + ^{90,92}\text{Zr}$ systems, it will be an interesting future work to extend our study presented in this article to three-dimensional calculations without resorting to the constant coupling approximation. This is so especially because the constant coupling approximation that we employed in this article may introduce a significant phase error and thus leads to an inconsistent angular-dependent interference between different partial waves. It may also be interesting to see whether this model accounts for the hindrance of fusion cross sections at deep sub-barrier energies recently found in several systems. For this purpose also, we would have

to take into consideration the coordinate dependence of the coupling form factor, especially around the touching point of the colliding nuclei [45].

ACKNOWLEDGMENTS

We thank E. Piasecki, M. Dasgupta, D. J. Hinde, M. Evers, and V. I. Zagrebaev for discussions. This work was supported by the Grant-in-Aid for Scientific Research (C), Contract No. 22540262 from the Japan Society for the Promotion of Science.

-
- [1] M. Dasgupta, D. J. Hinde, N. Rowley, and A. M. Stefanini, *Annu. Rev. Nucl. Part. Sci.* **48**, 401 (1998).
- [2] A. B. Balantekin and N. Takigawa, *Rev. Mod. Phys.* **70**, 77 (1998).
- [3] S. Ayik, B. Yilmaz, and D. Lacroix, *Phys. Rev. C* **81**, 034605 (2010).
- [4] N. Rowley, G. R. Satchler, and P. H. Stelson, *Phys. Lett. B* **254**, 25 (1991).
- [5] J. R. Leigh *et al.*, *Phys. Rev. C* **52**, 3151 (1995).
- [6] H. Timmers, J. R. Leigh, M. Dasgupta, D. J. Hinde, R. C. Lemmon, J. C. Mein, C. R. Morton, J. O. Newton, and N. Rowley, *Nucl. Phys. A* **584**, 190 (1995).
- [7] K. Hagino and N. Rowley, *Phys. Rev. C* **69**, 054610 (2004).
- [8] M. Zamrun F. and K. Hagino, *Phys. Rev. C* **77**, 014606 (2008).
- [9] K. Hagino, N. Rowley, and A. T. Kruppa, *Comput. Phys. Commun.* **123**, 143 (1999).
- [10] C. H. Dasso, S. Landowne, and A. Winther, *Nucl. Phys. A* **405**, 381 (1983); **407**, 221 (1983).
- [11] K. Hagino, N. Takigawa, and A. B. Balantekin, *Phys. Rev. C* **56**, 2104 (1997).
- [12] M. A. Nagarajan, A. B. Balantekin, and N. Takigawa, *Phys. Rev. C* **34**, 894 (1986).
- [13] J. O. Newton, R. D. Butt, M. Dasgupta, D. J. Hinde, I. I. Gontchar, C. R. Morton, and K. Hagino, *Phys. Rev. C* **70**, 024605 (2004).
- [14] C. L. Jiang *et al.*, *Phys. Rev. Lett.* **89**, 052701 (2002); C. L. Jiang, K. E. Rehm, B. B. Back, and R. V. F. Janssens, *Phys. Rev. C* **79**, 044601 (2009), and references therein.
- [15] M. Dasgupta, D. J. Hinde, A. Diaz-Torres, B. Bouriquet, C. I. Low, G. J. Milburn, and J. O. Newton, *Phys. Rev. Lett.* **99**, 192701 (2007).
- [16] A. M. Stefanini *et al.*, *Phys. Rev. C* **78**, 044607 (2008); *Phys. Lett. B* **679**, 95 (2009).
- [17] E. Piasecki *et al.*, *Phys. Rev. C* **80**, 054613 (2009).
- [18] Brookhaven National Laboratory, Evaluated Nuclear Structure Data File [<http://www.nndc.bnl.gov/ensdf/>], and references therein.
- [19] S. Raman, T. A. Walkiewicz, S. Kahane, E. T. Jurney, J. Sa, Z. Gacsi, J. L. Weil, K. Allaart, G. Bonsignori, and J. F. Shriner Jr., *Phys. Rev. C* **43**, 521 (1991).
- [20] A. V. Ignatyuk, J. L. Weil, S. Raman, and S. Kahane, *Phys. Rev. C* **47**, 1504 (1993).
- [21] A. Diaz-Torres, D. J. Hinde, M. Dasgupta, G. J. Milburn, and J. A. Tostevin, *Phys. Rev. C* **78**, 064604 (2008).
- [22] D. Agassi, C. M. Ko, and H. A. Weidenmüller, *Ann. Phys.* **107**, 140 (1977).
- [23] C. M. Ko, D. Agassi, and H. A. Weidenmüller, *Ann. Phys.* **117**, 237 (1979).
- [24] D. Agassi, C. M. Ko, and H. A. Weidenmüller, *Ann. Phys.* **117**, 407 (1979).
- [25] D. Agassi, C. M. Ko, and H. A. Weidenmüller, *Phys. Rev. C* **18**, 223 (1978).
- [26] V. I. Zagrebaev, *Ann. Phys. (NY)* **197**, 33 (1990).
- [27] T. Papenbrock and H. A. Weidenmüller, *Rev. Mod. Phys.* **79**, 997 (2007).
- [28] H. A. Weidenmüller and G. E. Mitchell, *Rev. Mod. Phys.* **81**, 539 (2009).
- [29] G. E. Mitchell, A. Richter, and H. A. Weidenmüller, *arXiv:1001.2422* [nucl-th], *Rev. Mod. Phys.* (in press).
- [30] C. W. J. Beenakker, *Rev. Mod. Phys.* **69**, 731 (1997).
- [31] D. M. Brink, J. Neto, and H. A. Weidenmüller, *Phys. Lett. B* **80**, 170 (1979).
- [32] N. Takigawa, K. Niita, Y. Okuhara, and S. Yoshida, *Nucl. Phys. A* **371**, 130 (1981).
- [33] K. Niita and N. Takigawa, *Nucl. Phys. A* **397**, 141 (1983).
- [34] M. Wilkinson, *Phys. Rev. A* **41**, 4645 (1990).
- [35] A. Bulgac, G. Do Dang, and D. Kusnezov, *Phys. Rev. E* **54**, 3468 (1996).
- [36] S. Mizutori and S. Aberg, *Phys. Rev. E* **56**, 6311 (1997).
- [37] C. M. Ko, H. J. Pimer, and H. A. Weidenmüller, *Phys. Lett. B* **62**, 248 (1976).
- [38] M. C. Nemes, *Nucl. Phys. A* **315**, 457 (1979).
- [39] R. Lipperheide, *Nucl. Phys. A* **260**, 292 (1976).
- [40] A. K. Kerman and S. E. Koonin, *Phys. Scr. A* **10**, 118 (1974).
- [41] N. Takigawa, K. Hagino, M. Abe, and A. B. Balantekin, *Phys. Rev. C* **49**, 2630 (1994).
- [42] M. Evers, M. Dasgupta, D. J. Hinde, L. R. Gasques, M. L. Brown, R. Rafiei, and R. G. Thomas, *Phys. Rev. C* **78**, 034614 (2008).
- [43] C. J. Lin, H. M. Jia, H. Q. Zhang, F. Yang, X. X. Xu, F. Jia, Z. H. Liu, and K. Hagino, *Phys. Rev. C* **79**, 064603 (2009).
- [44] M. V. Andres, N. Rowley, and M. A. Nagarajan, *Phys. Lett. B* **202**, 292 (1988).
- [45] T. Ichikawa, K. Hagino, and A. Iwamoto, *Phys. Rev. C* **75**, 057603 (2007); **75**, 064612 (2007); *Phys. Rev. Lett.* **103**, 202701 (2009).